Tropical Intraseasonal Oscillations Appearing in a GFDL General Circulation Model and FGGE Data. Part II: Structure

Y. HAYASHI AND D. G. GOLDER

Geophysical Fluid Dynamics Laboratory/NOAA, Princeton University, Princeton, New Jersey

(Manuscript received 21 December 1987, in final form 16 May 1988)

ABSTRACT

Space–time spectral and filter analyses are made of the structure of the tropical intraseasonal oscillations appearing in a GFDL 30-wavenumber spectral general circulation model and the FGGE IIIb data set.

The model's tropical zonal velocity exhibits spectral peaks with periods of 40–50 and 25–30 days at wavenumber 1 for six individual years, although the 40–50 day peak is not as pronounced as that found in the FGGE dataset. Both the eastward moving 40–50 and 25–30 day oscillations take the form of a Kelvin–Rossby wave pattern in the upper troposphere and a Rossby mode in the lower troposphere. They also take the form of a latitudinally tilted Walker cell which is modified by a meridional convergence in the boundary layer.

1. Introduction

In Part I (Hayashi and Golder 1986), space–time spectral and filter analyses were made of the tropical intraseasonal oscillations appearing in GFDL spectral general circulation models with rhomboidal wavenumber truncations at 30 and 15 and those appearing in the FGGE IIIb dataset during the northern summer (May–September). It was found that the 30-wavenumber model exhibited wavenumber 1 spectral peaks in the equatorial zone velocity at eastward moving periods of 40–50 and 25–30 days, although the 40–50 day peak was not as pronounced as that found in the FGGE data. Both these peaks were also detected in a conventional grid model with a resolution of 2.4 degrees. However, the 40–50 day peak was not clearly detected in the 15-wavenumber model, being consistent with the time spectral analysis of the same 15-wavenumber model by Lau and Lau (1986), who used 12 years of data.

These 40–50 and 25–30 day oscillations were characterized by a similar spatial structure in spite of the difference in their time scales. In particular, both of these oscillations exhibited a phase reversal between the upper and lower tropospheric zonal velocities, being consistent with the oscillation and propagation of the observed zonal–vertical cell (Fig. 1a) as suggested by Madden and Julian (1972). They found an eastward propagation with a node near the dateline and an antinode in the western hemisphere. Both the 40–50 and the 25–30 day wavenumber 1 precipitation oscillations were in phase with the vertical velocity and propagated eastward with major and minor antinodes in the eastern and western hemispheres, respectively. These oscillations also exhibited a meridional phase propagation, being consistent with the meridional propagation of the observed meridional–vertical cell (Fig. 1b) found in the monsoon region, as suggested by Yasunari (1981). Since these oscillations are associated with both zonal and meridional circulations, there is the possibility that the three-dimensional circulations may take the form of a combined Hadley–Walker cell (Fig. 1c) as suggested for the observed cold surge by Chang and Lau (1980). This circulation is similar to the observed intraseasonal divergent circulations (Lorenc 1984) which flow across the velocity potential contours (Fig. 1d). However, the velocity potential tends to smear the latitudinally narrow structure of an equatorially trapped mode, since it acts like a two-dimensional smoother (Hendon 1986). Moreover, the divergent circulation is accompanied by the nondivergent circulation. It was also shown in Part I that the wavenumber 1 pattern of the 40–50 and 25–30 day oscillations at 200 mb had the form of a Kelvin mode near the equator and a Rossby mode away from the equator. The Rossby mode is associated with a meridional wind component that is highly nondivergent (i.e., rotational). This nondivergent component will complicate the three-dimensional circulation.

The present paper (Part II), which is an extension of Part I (Hayashi and Golder 1986) confirms the existence of the 40–50 and 25–30 day oscillations in the 30-wavenumber model for different years and gives a more comprehensive three-dimensional structure of these oscillations.

Corresponding author address: Dr. Yoshikazu Hayashi, Geophysical Fluid Dynamics Laboratory, Princeton University, P.O. Box 308, Princeton, NJ 08542.

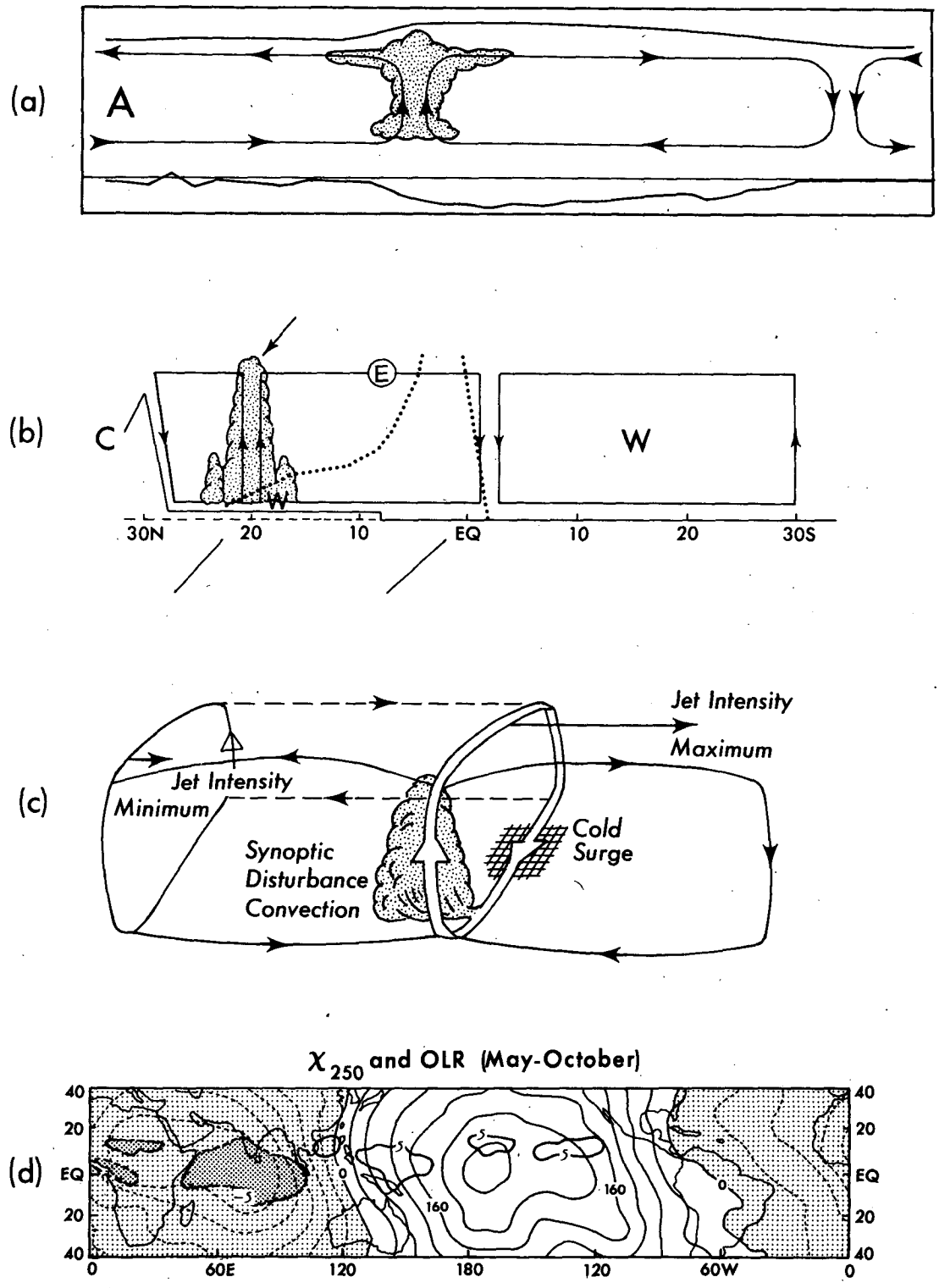

FIG. 1. Schematic of (a) the zonal–vertical (Walker) cell associated with the observed tropical intraseasonal oscillation (after Madden and Julian 1972, a panel of Fig. 16). (b) As in (a) but of the meridional–vertical (Hadley) cell associated with the observed tropical intraseasonal oscillation in the monsoon region (after Yasunari, 1981 a panel of Fig. 19). (c) As in (a) but of the combined Hadley–Walker cell associated with the winter monsoon cold surge (after Chang and Lau 1980, a panel of Fig. 14). (d) Composite 250 mb velocity potential anomalies (light contours and shading) with the composite outgoing longwave radiation anomalies (dark contours with dark shading for negative regions) (after Knutson and Weickmann 1987, a panel of Fig. 6a).

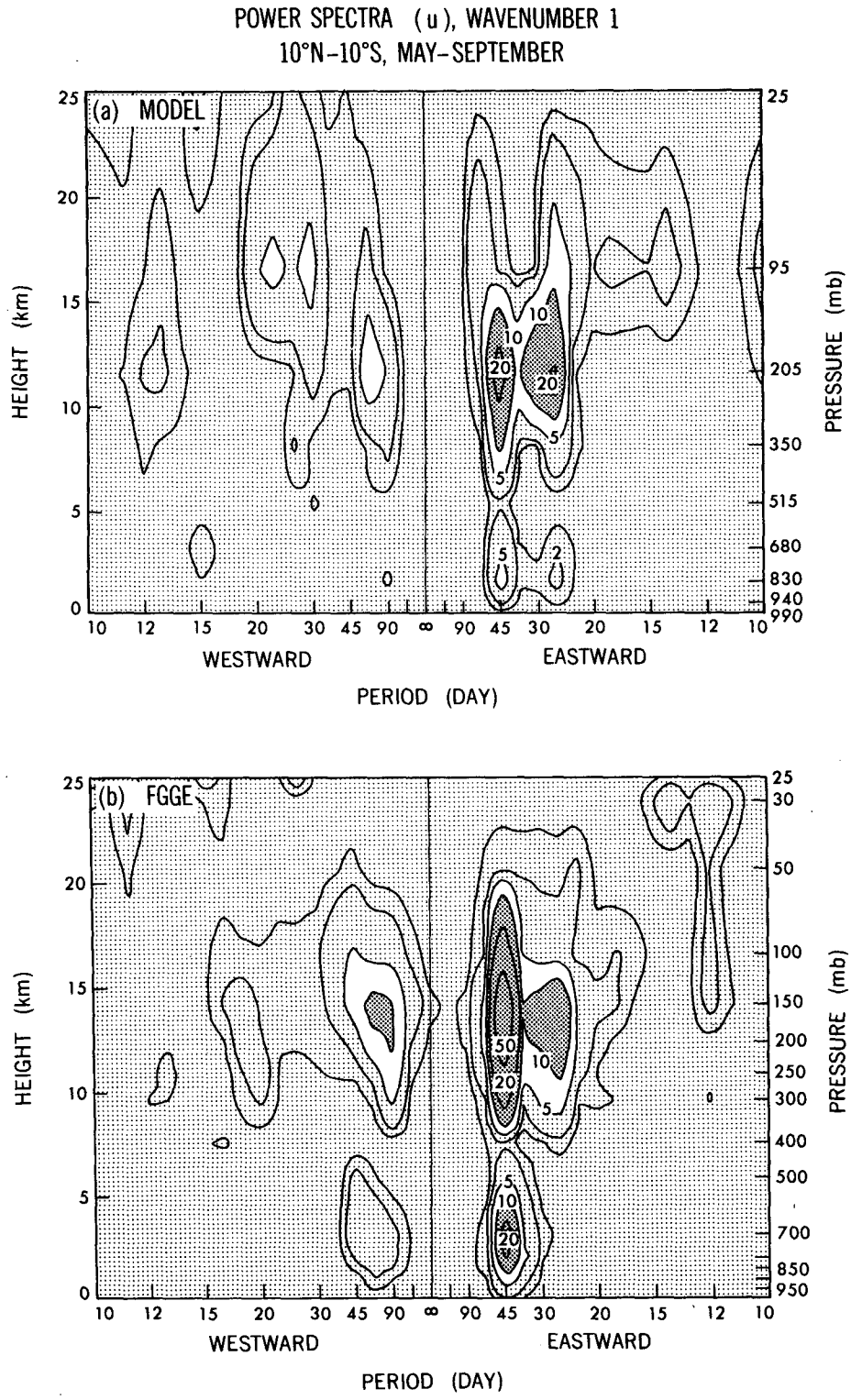

FIG. 2. Frequency–height distribution (wavenumber 1, May–September) of the space-time power spectral density (10 m^2 s^{-2} day) of the zonal velocity (10°N–10°S average) of (a) the model and (b) the FGGE. Contours 1, 2, 5, 10, 20. Dark shade >10, light shade <5.

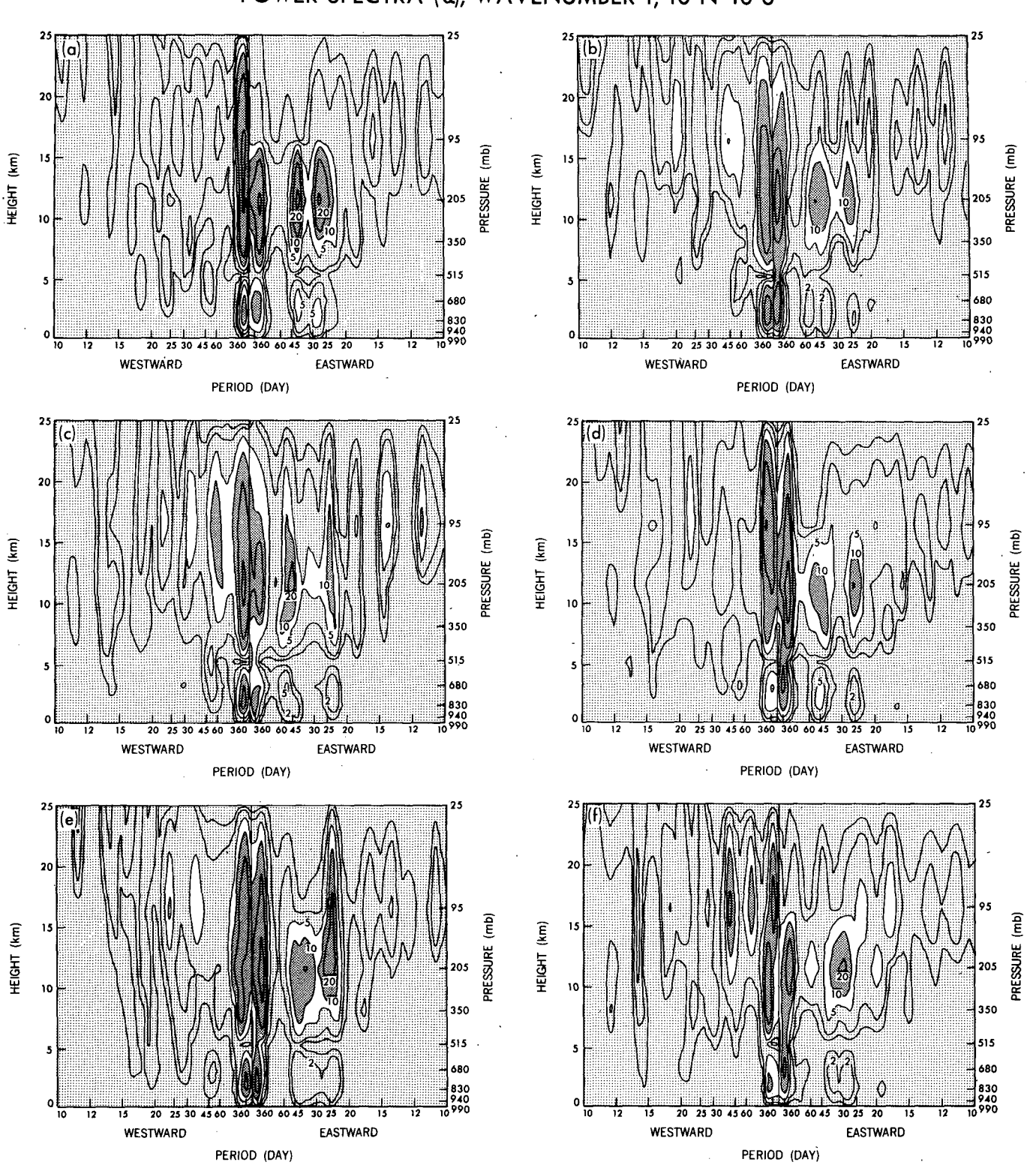

FIG. 3. Frequency–height distributions (wavenumber 1) of the space-time power spectral density (10 $m^2 s^{-2}$ day) of the zonal velocity (10°N–10°S) of the model for six individual years (a, b, c, d, e). Contours 1, 2, 5, 10, 20, 50. Dark shade >10, light shade <5.

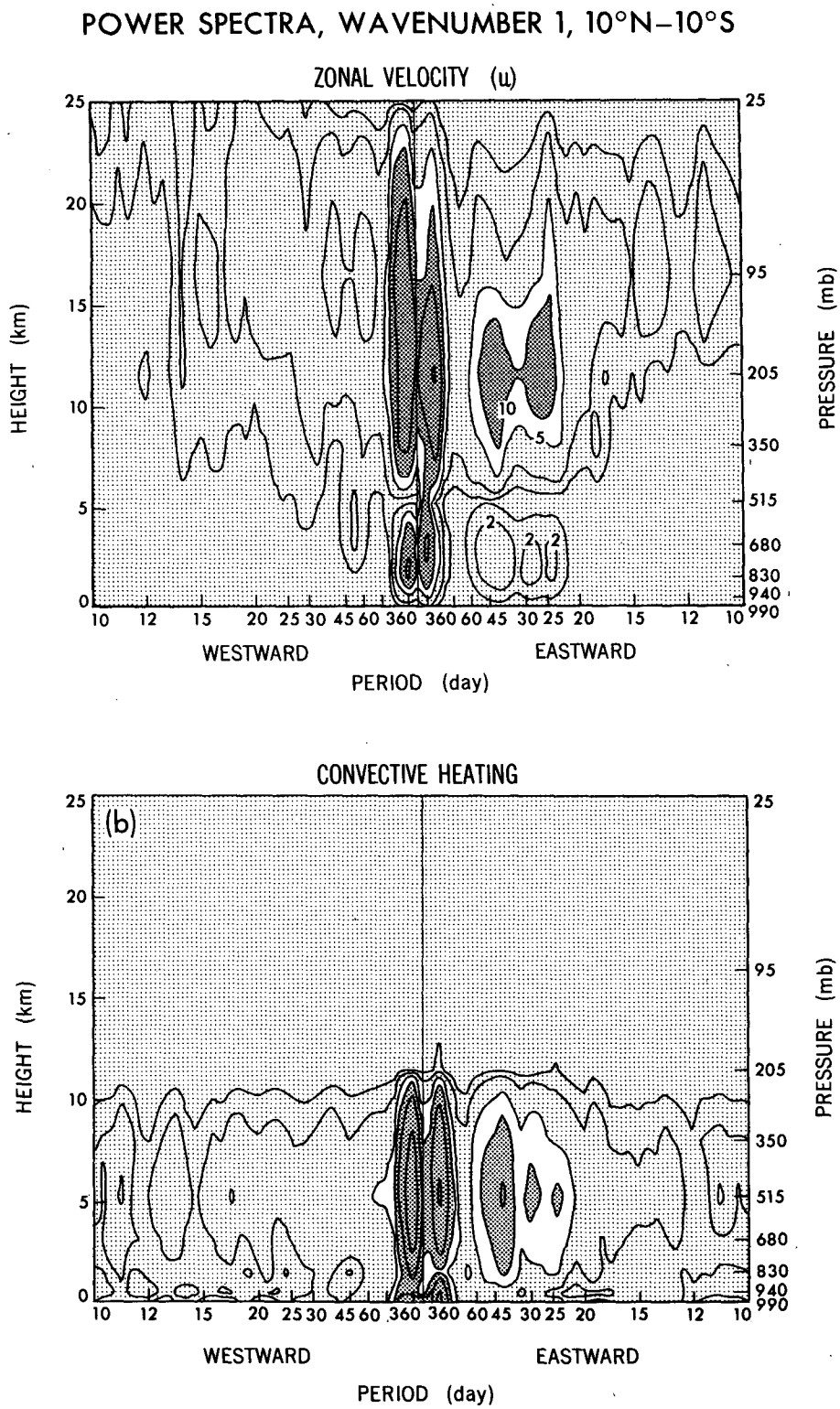

FIG. 4. Frequency–height distributions (wavenumber 1) of (a) the space–time power spectral density ($10\ m^2\ s^{-2}$ day) of the zonal velocity (10°N–10°S) of the model for 6 entire years. Contours 1, 2, 5, 10, 20, 50. Dark shade >10, light shade <5. (b) As in (a) except for convective heating ($10^{-2}\ K^2\ s^{-2}$, day). Contours 10, 20, 50, 100, 200, 500. Dark shade >100, light shade <50.

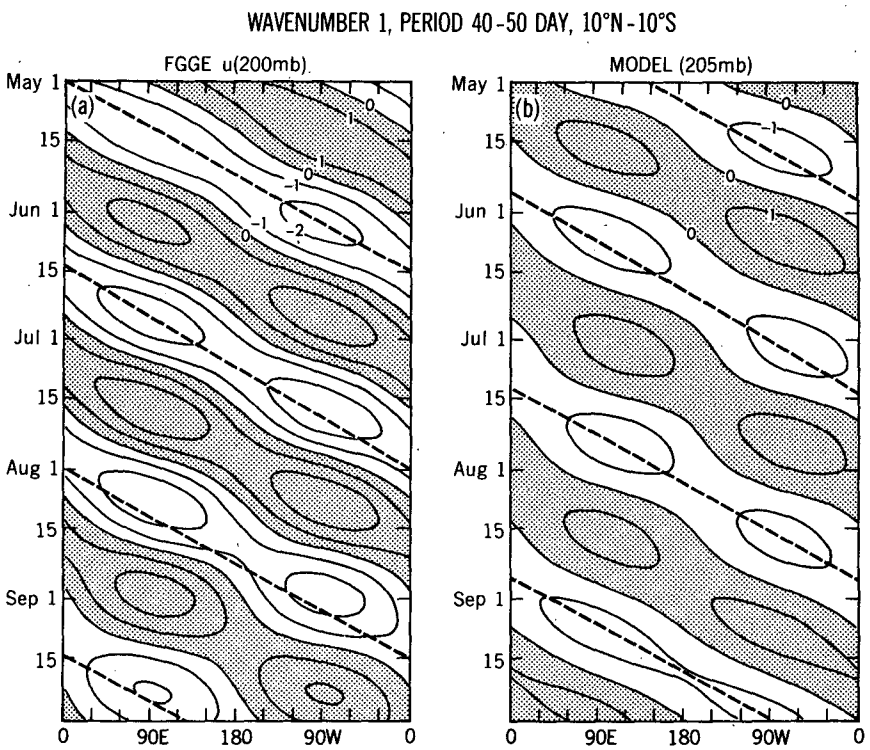

FIG. 5. Longitude–time distributions (10°N–10°S average) of the frequency-filtered (40–50 day) wavenumber 1 zonal velocity. (a) FGGE at 200 mb, (b) model at 205 mb. Slanted straight lines indicate the phase speed of 10.3 m s^{-1}. Contour interval 1 m s^{-1}. Dark shade >0.

2. Space–time spectral and filter analyses

In the present analysis, the spectral distributions are given by space–time spectra estimated by the maximum entropy method (see Hayashi 1982), while the propagation and structure are obtained by a recursive time filter (See Murakami 1979). Only the FGGE data corresponding to the model's vertical resolution (below 25 mb) are used in this study.

a. Spectral distribution

Figure 2 shows the frequency–height distributions (May–September) of the space–time power spectra (wavenumber 1) of the zonal velocity of the model and the FGGE data, which are averaged over 10°N to 10°S. The seasonal variation has been removed by subtracting monthly means from the original once-daily data. It is seen that the model's zonal velocity (Fig. 2a) exhibits spectral peaks at periods of 40–50 and 25–30 days, although the 40–50 day peak is not as pronounced as that occurring in FGGE (Fig. 2b).

In order to examine whether these two peaks appear during different model years, Fig. 3 gives the frequency–height distributions (over an entire year) of the space–time power spectra (wavenumber 1) for the zonal velocity (10°N–10°S average) during six individual model years. For these spectra, the seasonal variation has not been subtracted from the original data. It should be noted that both 40–50 and 25–30 day peaks appear distinctly every year except for the sixth year (Fig. 3f) in which these peaks merge in the upper troposphere. Interestingly, the annual oscillation is biased toward an eastward moving component. This annual oscillation is a modulation of the stationary (i.e., annual mean) component which is subtracted from the original data prior to the spectral computation.

Figure 4 shows the frequency–height distributions (6 year average) of the space–time power spectra (wavenumber 1) of zonal velocity (a) and convective heating (b) of the model (10°N–10°S average). Both 40–50 and 25–30 day peaks occur in the six year spectra. Both 40–50 day and 25–30 day convective heating oscillations attain their maximum amplitude at 515 mb and are confined to the troposphere. It is of theoretical importance to note that the 40–50 and 25–30 day periods are not due to different vertical distributions of convective heating. For example, the period of wave-CISK increases with increase in the low level heating for the same heating in the upper level (Takahashi 1987).

b. Propagation and structure

The zonal propagation of the wavenumber 1 component is visualized by Fig. 5 which shows longitude–

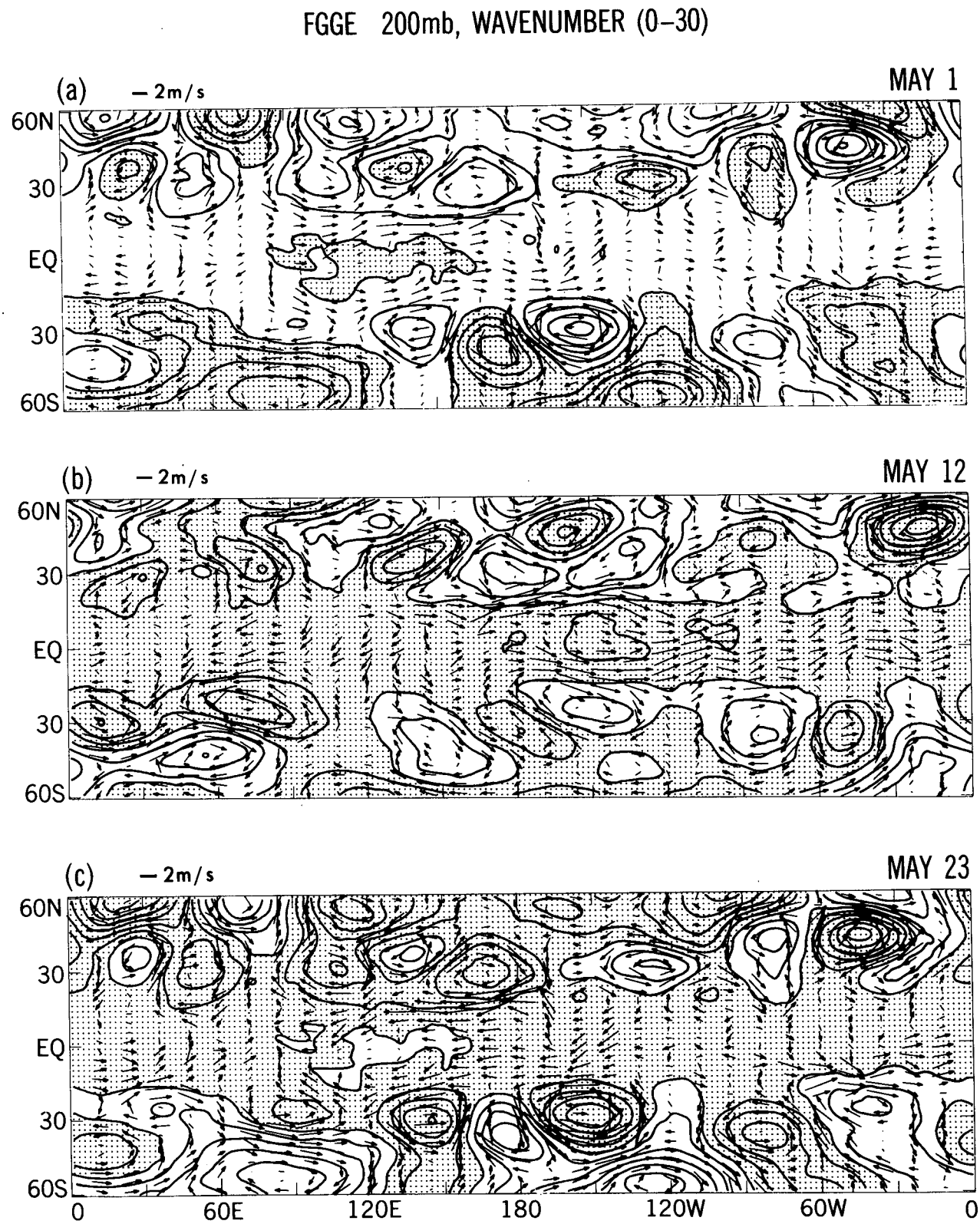

FIG. 6. Longitude–latitude sections (FGGE, 200 mb) of 40–50 day filtered wind vectors and geopotential height contours on (a) 1, (b) 12, and (c) 23 May 1979. Contour interval 10 m. Shading indicates positive values.

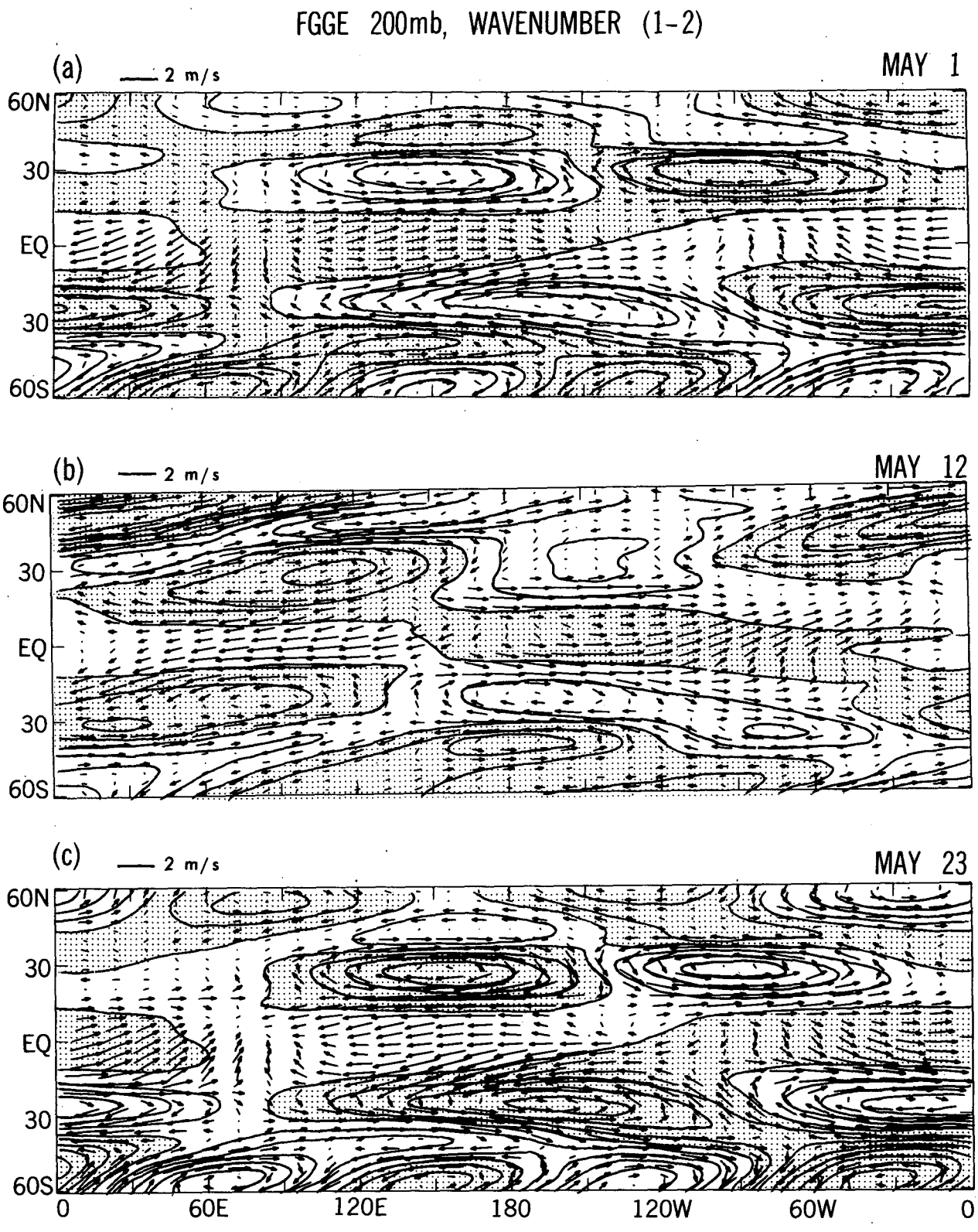

FIG. 7. As in Fig. 6 except for wavenumber 1–2 components. Contour interval 5 m.

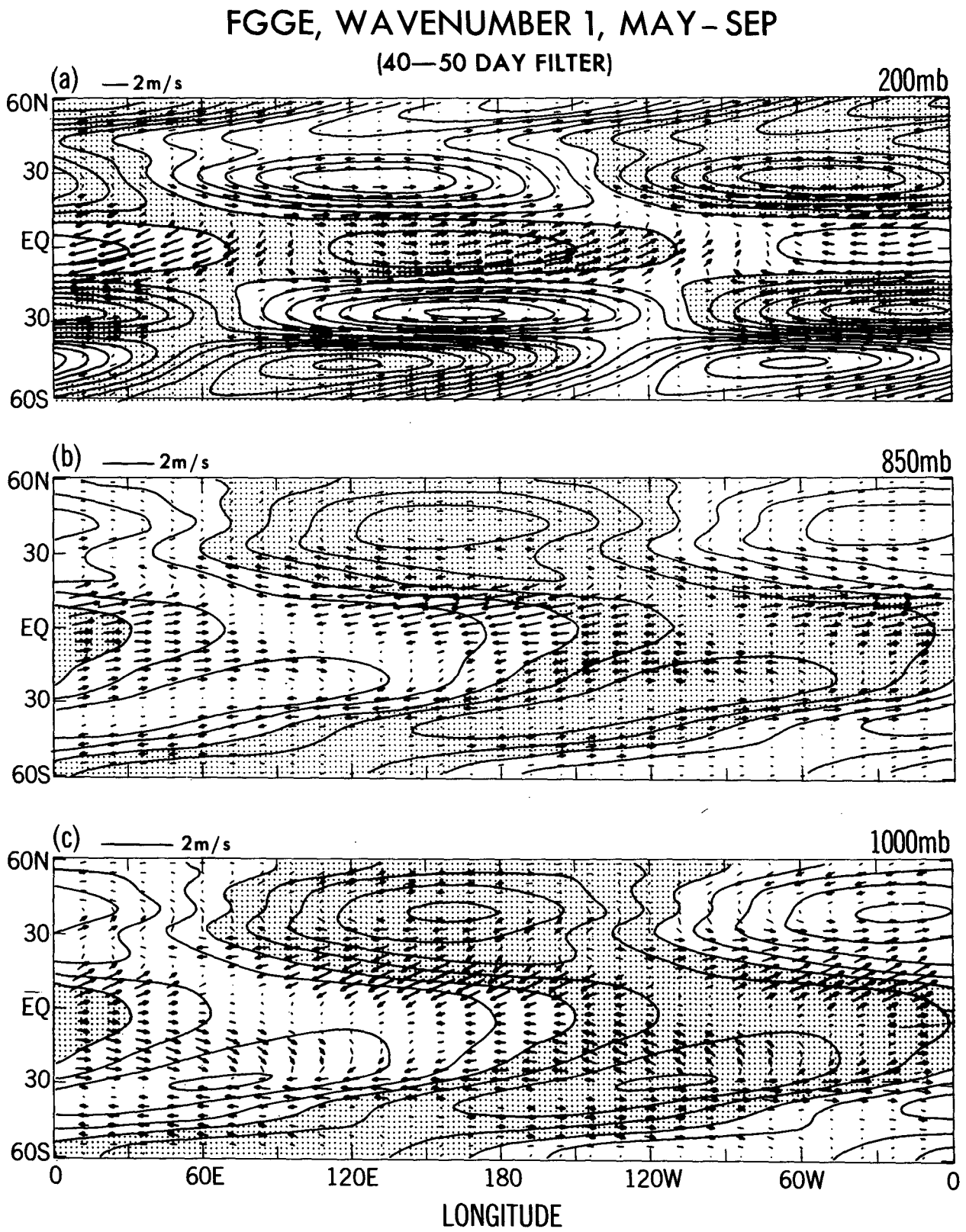

FIG. 8. Longitude–latitude sections (FGGE) at (a) 200 mb, (b) 850 mb and (c) 1000 mb of the wavenumber 1, 40–50 day filtered wind vectors and geopotential height contours which are composited over May–September along the longitude-time isolines of the phase velocity (10.3 m s^{-1}) of the 40–50 day oscillation. Contour interval 2 m. Shading indicates positive values.

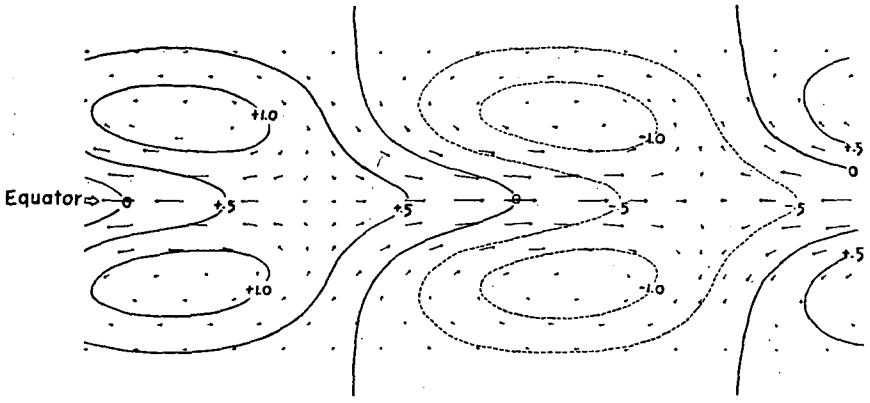

FIG. 9. Horizontal pattern (wind vectors and pressure contours) of stationary circulation caused by the heat source and sink (reproduced from Matsuno 1966, Fig. 9).

time distributions (10°N–10°S average) of the frequency-filtered (40–50 day) wavenumber 1 zonal velocities of the FGGE data (200 mb) and the model (205 mb). These wavenumber 1 components propagate eastward with nodes occurring at 0° and 180° longitude due to an interference between the eastward and westward moving components. The eastward phase speed of 10.3 m s^{-1} (corresponding to a 45-day period) is indicated by slanted lines.

Figure 6 shows longitude–latitude sections (FGGE, 200 mb) of the wind vectors and geopotential height contours on the 1st (a), 12th (b), and 23rd (c) of May. Both the wind and geopotential height consist of all resolvable wavenumbers (0–30) but were subjected to a 40–50 day time filter. Near the equator, the wind vectors are dominated by a wavenumber 1 component, while the geopotential height is dominated by a wavenumber 0 (zonal mean) component. The wind vectors clearly indicate an eastward phase propagation. However, it is difficult to detect an eastward propagation of the geopotential height which pulsates with the dominant wavenumber 0 component.

Figure 7 is the same as Fig. 6 except for the wavenumber 1–2 components. In the tropics, the eastward propagation of the wavenumber 1 zonal velocity and geopotential height are clearly seen. At 60°S, a pulsation of wavenumber 2 patterns can be seen.

Figure 8 displays longitude–latitude sections (FGGE, 200 mb, 850 mb, 1000 mb) of wavenumber 1, 40–50 day filtered wind vectors and geopotential height contours which have been composited daily over the period May–September along the longitude–time isoline (see Fig. 7) of the eastward phase velocity (10.3 m s^{-1}) corresponding to a 40–50 day period oscillation. This space–time composite enhances the eastward moving component and reduces the westward moving component. The longitudes of this composite are intended to indicate the longitudinal separation and not to specify the position of moving wave patterns at a particular time. At 200 mb (Fig. 8a), the wind vectors near the equator are parallel to the equator, while the zonal velocity attains its maximum amplitude over the equator and is in phase with the geopotential height, being consistent with the Kelvin mode (see Fig. 8 of Matsuno 1966). However, the geopotential height reverses its phase across 15°N, being inconsistent with the Kelvin mode. The wave pattern around 30°N resembles an equatorial Rossby mode (see Fig. 4 of Matsuno 1966) in that the wind vectors geostrophically follow the geopotential height contours. This pattern propagates eastward as can be seen in Fig. 7, being contrary to a free Rossby mode which propagates westward. The eastward propagation strongly suggests that the 40–50 day oscillation is a forced oscillation. At the 850 mb (Fig. 8b), the geopotential height is characterized by a Rossby mode which attains its maximum zonal component away from the equator and is associated with geostrophic wind vectors. At 1000 mb (Fig. 8c), the wave pattern is associated with ageostrophic wind vectors, probably due to the Ekman drift. These wave patterns are similar to that (Fig. 9) of the thermally forced stationary and low frequency equatorial waves of the two-dimensional theoretical models of Matsuno (1966), Gill (1980), and Yamagata and Hayashi (1984).

Figures 10 and 11 show the composited wave patterns of the model's 40–50 and 25–30 day oscillations which are subjected to 40–50 and 25–30 day filters, respectively. As in the FGGE 40–50 day oscillation, both these oscillations take the form of a Kelvin–Rossby wave pattern in the upper troposphere with a maximum zonal component occurring at the equator, while they take the form of a Rossby wave pattern in the lower troposphere with a maximum zonal component occurring away from the equator.

Figure 12a shows longitude–latitude sections (FGGE) of the contours of the 40–50 day composited vertical velocity at 500 mb and the wind vectors at 200 mb. The 500 mb vertical velocity can be interpreted as a measure of the horizontal convergence at 200 mb

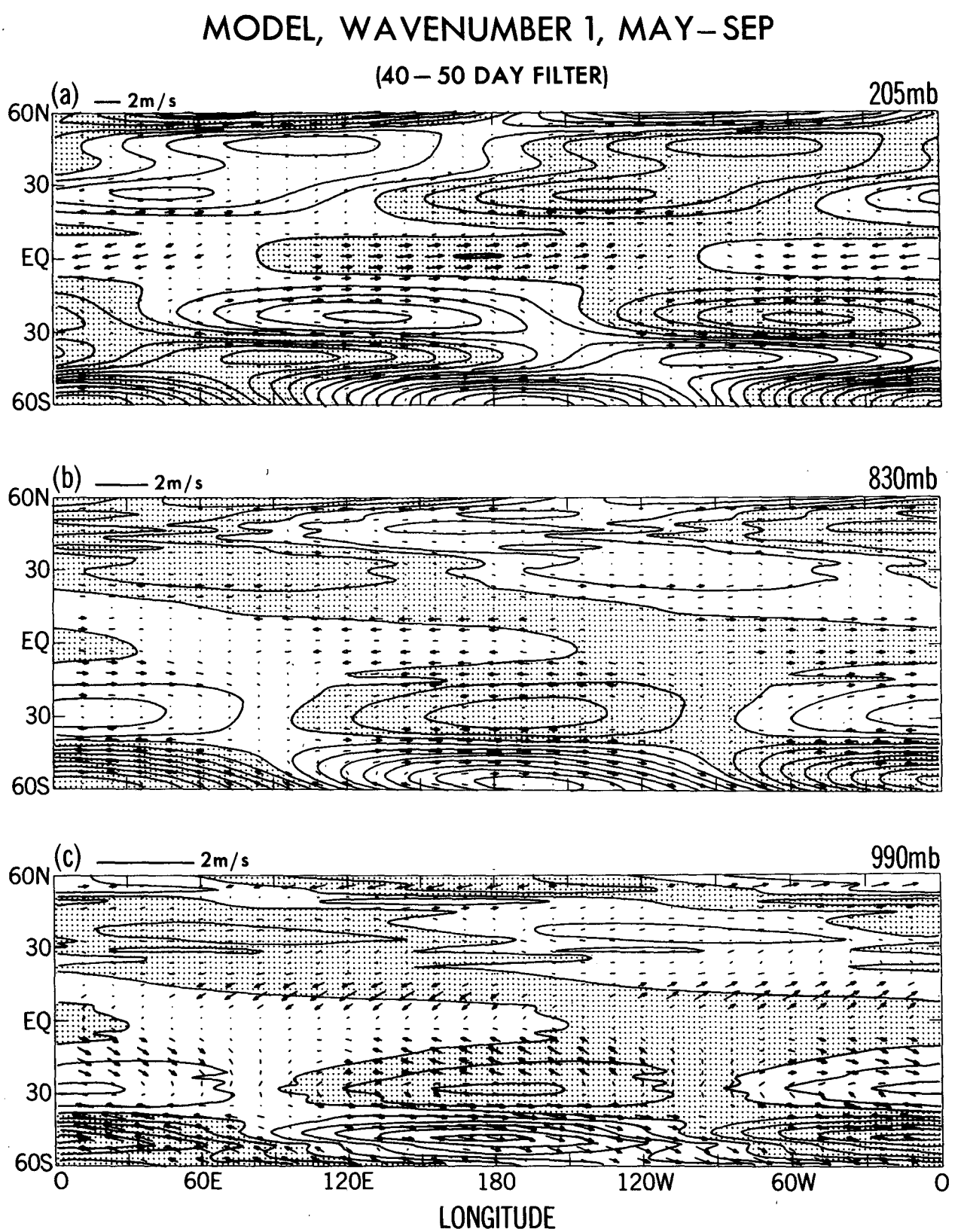

FIG. 10. Longitude–latitude sections (model) at (a) 205 mb, (b) 830 mb, (c) 990 mb of the wavenumber 1, 40–50 day filtered wind vectors and geopotential height contours which are composited over May–September along the longitude–time isoline (see Fig. 4b) of the eastward phase velocity (10.3 m s^{-1}) of the 40–50 day oscillations. The origin of longitude has been shifted toward the west by 138°. Contour intervals 2 m. Shading indicates positive values.

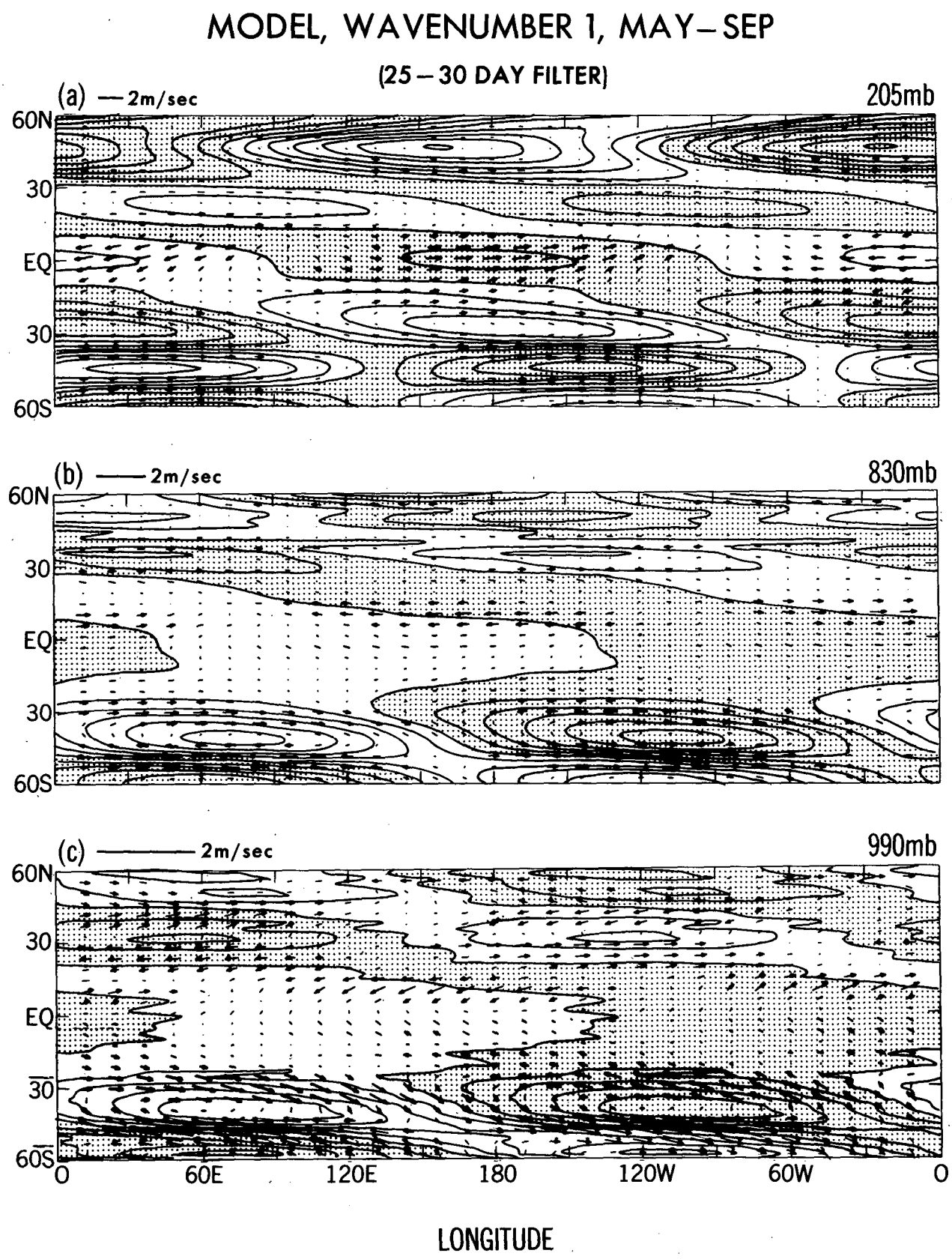

FIG. 11. As in Fig. 10 except for 25–30 day filter and eastward phase velocity of 16.8 m s^{-1}. Contour intervals 2 m s^{-1}.

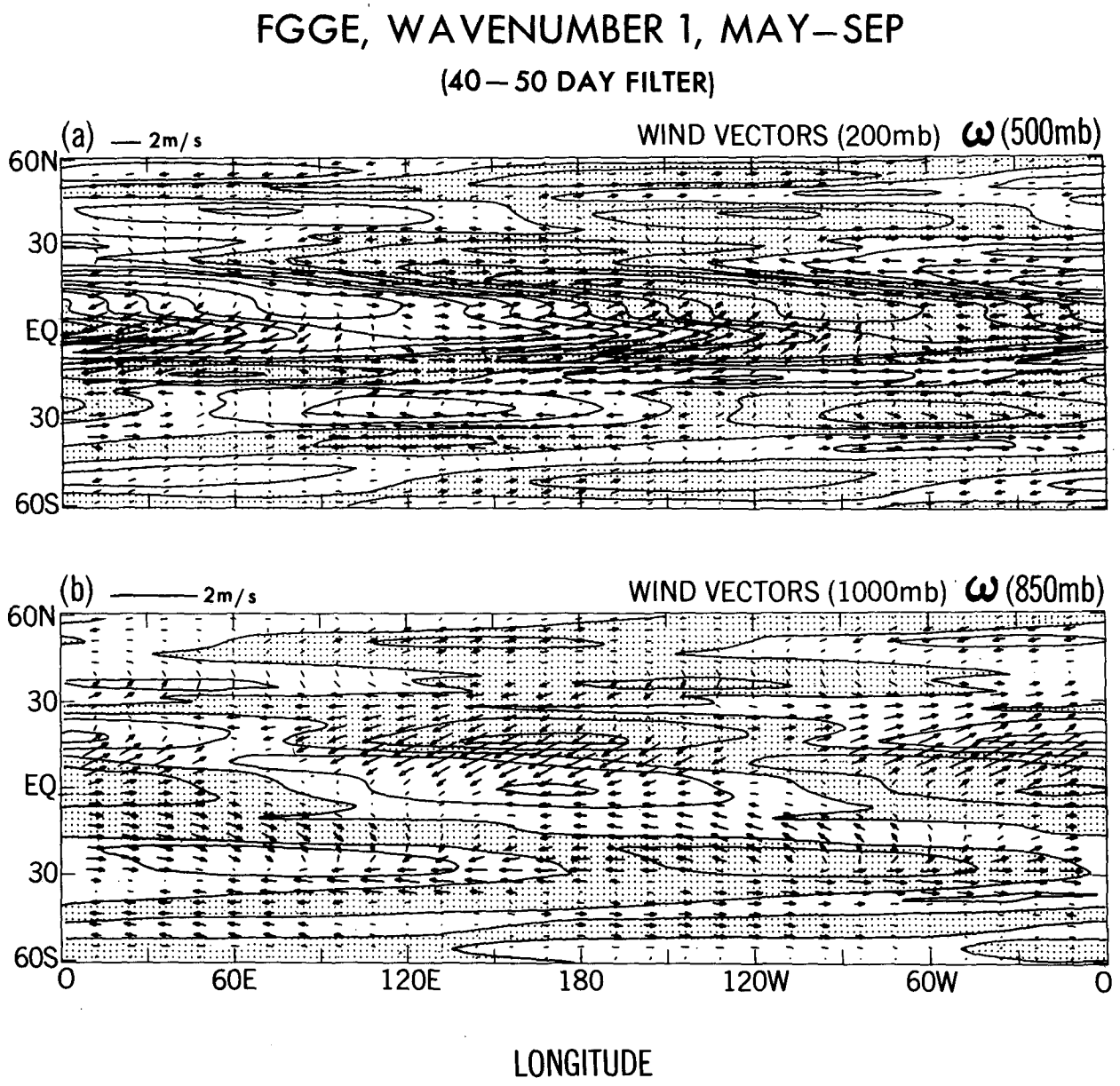

FIG. 12. Longitude–latitude section (FGGE) of the contours of wavenumber 1, 40–50 day filtered composite vertical pressure velocity at (a) 500 mb and (b) 850 mb, and wind vectors at (a) 200 mb and (b) 1000 mb. Contour intervals 2×10^{-11} Pa s^{-1}. Shading indicates downward motion.

due to the continuity of mass. It is seen that the horizontal convergence is consistent with that of the Walker cell, which is associated with a zonal convergence as observationally suggested by Madden and Julian (1972). It should be noted, however, that the vertical velocity is associated with a northwest–southeast tilt between 0° and 20°N. This meridional tilt results in a northward phase propagation of the eastward propagating vertical velocity as demonstrated in Part I (Hayashi and Golder 1986, Fig. 13). The short meridional scale of divergence can hardly be detected in the observed velocity potential (Lorenc 1984; Krishnamurti et al. 1985), which acts like a two-dimensional smoother.

Figure 12b is the same as Fig. 12a except that it shows the vertical velocity at 850 mb and the wind vectors at 1000 mb. The 850 mb vertical velocity can be interpreted as a measure of the horizontal convergence at 1000 mb. It is seen that the horizontal convergence is largely modified by a meridional convergence. In particular, the vertical velocity at 850 mb is not 90 degrees out of phase with the zonal velocity at 1000 mb, being inconsistent with the Walker cell. This meridional velocity is probably due mainly to the Ek-

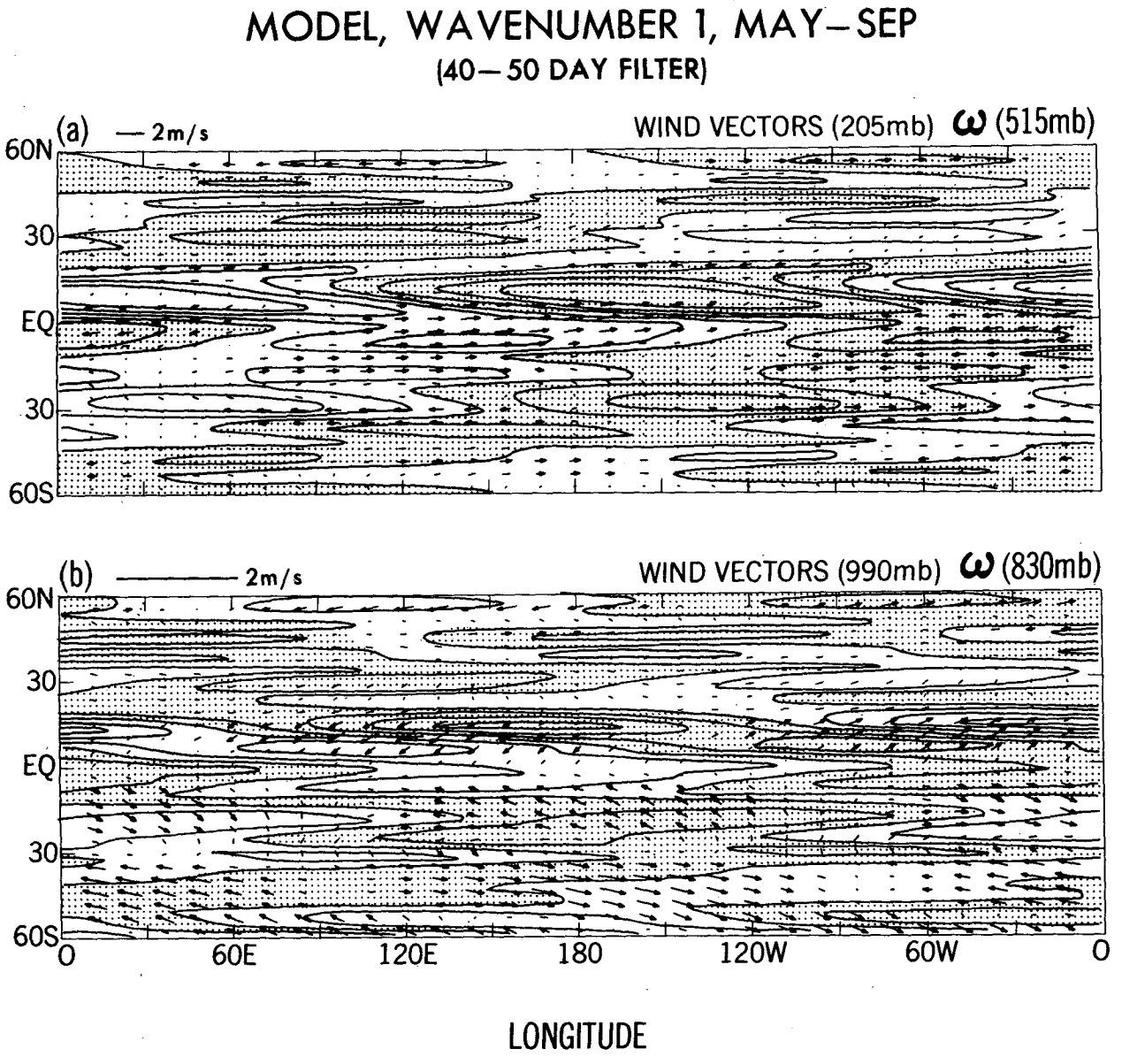

FIG. 13. Longitude–latitude section (model) of the contours of 40–50 day filtered composite vertical pressure velocity at (a) 515 mb and (b) 830 mb and wind vectors at (a) 205 mb and (b) 990 mb. Shading indicates downward motion.

man drift, since the wind vectors do not follow the geopotential height contours as was illustrated in Fig. 8c.

Figures 13 and 14 show the composited vertical velocity patterns of the model's 40–50 and 25–30 day oscillations. The quadrature phase relation between the zonal velocity at 205 mb and the vertical velocity at 515 mb is not as clear as that of the FGGE 40–50 day oscillation, respectively. This defect is probably because the 40–50 and 25–30 day oscillations coexisting in the model have some overlapping in their frequency spectral distributions. The boundary layer convergence of the 40–50 and 25–30 day oscillations is largely modified by a meridional convergence, being in agreement with the FGGE 40–50 day oscillation. Also, the vertical velocity exhibits a northwest–southeast tilt between the equator and 20°N.

Figure 15 schematically extracts from Figs. 12, 13 and 14 the essential features of the three-dimensional circulation of the eastward moving wavenumber 1 component (shown as a half-wavelength) of the tropical 40–50 and 25–30 day oscillations, and illustrates that the oscillations take the form of Walker cells with a northwest–southeast tilt between 0°–20°N. It also in-

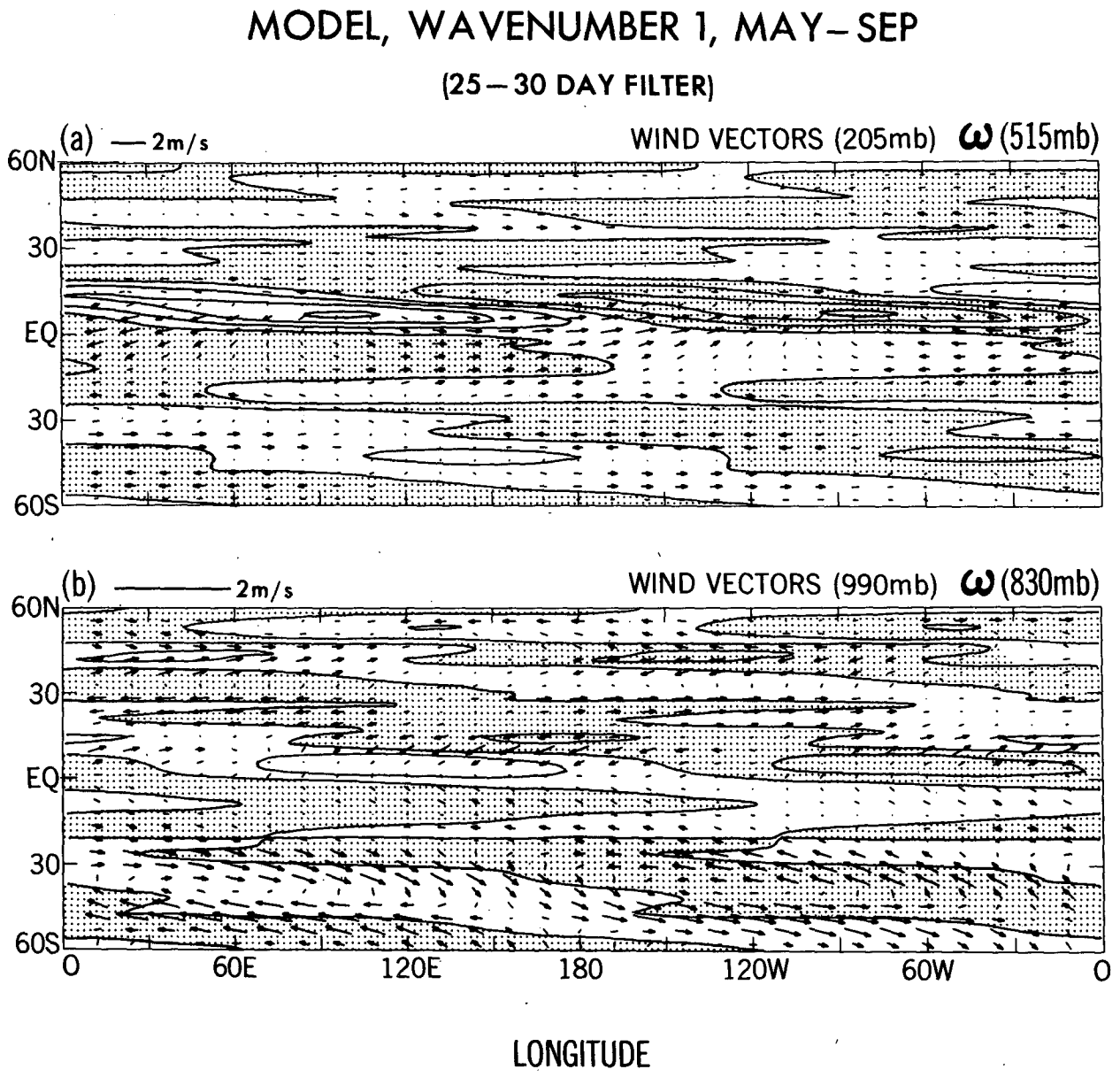

FIG. 14. As in Fig. 13 except for 25–30 day filter and eastward phase velocity of 16.8 m s^{-1}.

dicates that the vertical velocity at 500 mb is 90 degrees out of phase with the zonal velocity at 200 and 800 mb. Although it is not illustrated schematically, the vertical velocity at 800 mb is not 90 degrees out of phase with the zonal velocity at 800 mb due to the meridional convergence in the boundary layer. This is due to the fact that the Walker cell in the boundary layer cannot be strictly described by a continuous zonal–vertical streamline but is represented by many vectors intersecting this approximate streamline (not illustrated). It is difficult to illustrate the meridional velocity schematically, since it does not strictly take the form of a local Hadley cell as suggested by Yasunari (1981) and Murakami et al. (1984, Fig. 16) due to the presence of the associated zonal velocity. In this respect, the structure of the tropical 40–50 and 25–30 day oscillations is more complex than that of the winter monsoon cold surge which is characterized by a strong meridional velocity, as was schematically illustrated by Fig. 1c (after Chang and Lau 1980) in the Introduction. There is no direct flow linking the upward and downward motion, since the divergent flow is accompanied by the nondivergent flow associated with the Rossby mode.

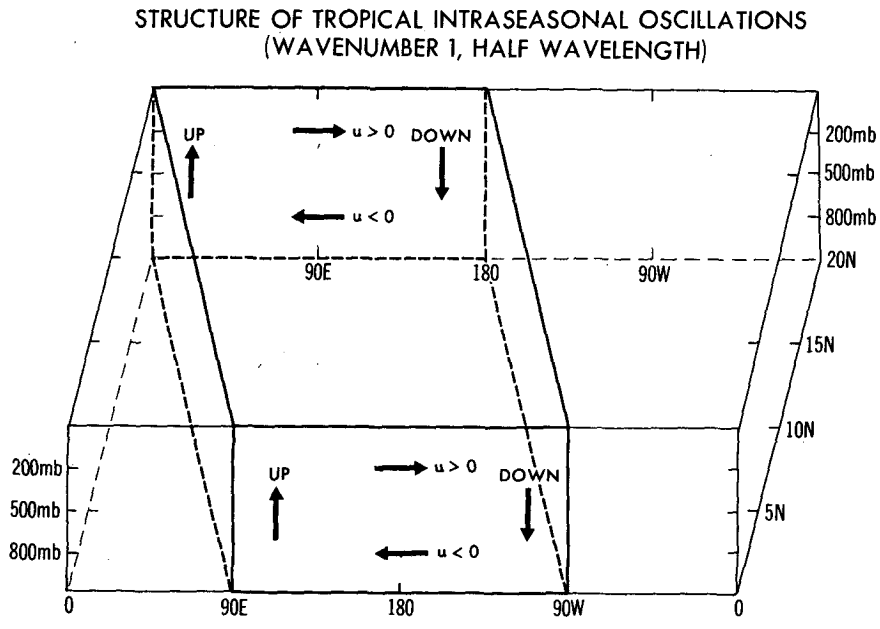

FIG. 15. Schematic three-dimensional circulations (wavenumber 1, half-wavelength) of tropical 40–50 and 25–30 day oscillations. Horizontal and vertical arrows indicate zonal and vertical velocities, respectively. The low level velocity involves a strong meridional velocity (not illustrated).

3. Conclusions and remarks

The present paper (Part II) has made a comprehensive study of the structure of the tropical intraseasonal oscillations appearing in a GFDL 30-wavenumber spectral model and the FGGE data processed at GFDL. The main conclusions are summarized as follows.

1) The model's tropical zonal velocity exhibits spectral peaks with periods of 40–50 and 25–30 days at wavenumber 1 for 6 individual years, although the 40–50 day peak is not as pronounced as that found in the FGGE dataset.

2) Both 40–50 and 25–30 day oscillations take the form of a Kelvin–Rossby wave pattern in the upper troposphere and a Rossby wave pattern in the lower troposphere. They also have the form of a Walker cell with a meridional tilt except that the horizontal convergence in the boundary layer is largely modified by a meridional convergence. They do not strictly take the form of a local Hadley cell, since the meridional component is accompanied by a strong zonal component.

Although the 40–50 day oscillations are reasonably well simulated by the model, the deficiency in their amplitude being less than that observed may have a serious effect on long-range forecasts in the tropics.

The propagation and structure of the tropical intraseasonal oscillations studied here can be reproduced rather well by a three-dimensional linear response model with a boundary layer (Hayashi and Miyahara 1987). The linear models with and without boundary layers confirm that the horizontal convergence in the boundary layer is largely modified by a frictional meridional convergence. The dominance of the Rossby mode in the lower troposphere is also due to the effect of surface friction, while the combined Kelvin–Rossby mode in the upper troposphere is a response to the eastward propagating thermal forcing. The frictional convergence will also affect the thermal forcing itself through moisture convergence.

Acknowledgments. The authors are grateful to Dr. S. Manabe for his valuable advice and to Drs. I. M. Held and N.-C. Lau and two anonymous reviewers for their appropriate comments on the original manuscript.

REFERENCES

Chang, C. P., and K. M. Lau, 1980: Northeasterly cold surges and near-equatorial disturbances over winter MONEX during December 1974. Part II: Planetary scale aspects. *Mon. Wea. Rev.*, **108**, 298–312.

Gill, A. E., 1980: Some simple solutions for heat-induced tropical circulations. *Quart. J. Roy. Meteor. Soc.*, **106**, 447–462.

Hayashi, Y., 1982: Space–time spectral analysis and its applications to atmospheric waves. *J. Meteor. Soc. Japan*, **60**, 156–171.

——, and D. G. Golder, 1986: Tropical intraseasonal oscillations appearing in a GFDL general circulation model and FGGE data, Part I: Phase propagation. *J. Atmos. Sci.*, **43**, 3058–3067.

——, and S. Miyahara, 1987: A three-dimensional linear response model of the tropical intraseasonal oscillation. *J. Meteor. Soc. Japan*, **65**, 843–857.

Hendon, H. H., 1986: Streamfunction and velocity potential representation of equatorially trapped waves. *J. Atmos. Sci.*, **43**, 3038–3042.

Knutson, T. R., and K. M. Weickmann, 1987: 30–60 day atmospheric oscillations: Composite life cycles of convection and circulation anomalies. *Mon. Wea. Rev.*, **115**, 1407–1436.

Krishnamurti, T. N., P. K. Jayakumar, J. Sheng, N. Surgi and A. Kumar, 1985: Divergent circulation on the 30 to 50 day time scale. *J. Atmos. Sci.*, **42**, 364–375.

Lau, N. C., and K. M. Lau, 1986: The structure and propagation of intraseasonal oscillations appearing in a GFDL GCM. *J. Atmos. Sci.*, **43**, 2023–2047.

Lorenc, A. C., 1984: The evolution of planetary scale 200 mb divergent flow during the FGGE year. *Quart. J. Roy. Meteor. Soc.*, **110**, 427–441.

Madden, R. A., and P. R. Julian, 1972: Description of global-scale circulation cells in the tropics with a 40–50 day period. *J. Atmos. Sci.*, **29**, 1109–1123.

Matsuno, T., 1966: Quasi-geostrophic motions in the equatorial area. *J. Meteor. Soc. Japan* **44**, 25–43.

Murakami, M., 1979: Large-scale aspects of deep convective activity over the GATE area. *Mon. Wea. Rev.*, **107**, 994–1013.

Murakami, T., T. Nakazawa and J. He, 1984: On the 40–50 day oscillations during the 1979 Northern Hemisphere summer. Part I: Phase propagation. *J. Meteor. Soc. Japan*, **62**, 440–468.

Takahashi, M., 1987: A theory of the slow phase speed of the intraseasonal oscillation using the wave-CISK. *J. Meteor. Soc., Japan* **65**, 43–49.

Yamagata, T., and Y. Hayashi, 1984: A simple diagnostic model for the 30–50 day oscillation in the tropics. *J. Meteor. Soc. Japan*, **62**, 709–717.

Yasunari, T., 1981: Structure of an Indian summer monsoon system with around 40-day period. *J. Meteor. Soc. Japan*, **59**, 336–354.